https://doi.org/10.5194/egusphere-2023-1428
Preprint. Discussion started: 11 August 2023

Quantifying the migration rate of drainage divides from high-resolution topographic data

Chao Zhou[1], Xibin Tan[2,*], Yiduo Liu[2], Feng Shi[1,3]

[1] State Key Laboratory of Earthquake Dynamics, Institute of Geology, China Earthquake Administration, Beijing 100029, China

[2] Key Laboratory of Mountain Hazards and Surface Processes, Institute of Mountain Hazards and Environment, Chinese Academy of Sciences, Chengdu 610299, China

[3] Shanxi Taiyuan Continental Rift Dynamics National Observation and Research Station, Beijing 100029, China

*Corresponding author. E-mail address: tanxibin@imde.ac.cn

Abstract

The lateral movement of drainage divides is co-influenced by tectonics, lithology, and climate, and therefore archives a wealth of geologic and climatic information. Several methods have been proposed to determine the direction of drainage-divide migration. However, how to quantify the migration rate of drainage divides remains challenging. Here, we propose a new approach to calculate the migration rate of drainage divides from high-resolution topographic data. The new method is based on the cross-divide comparison of channel-head parameters, including the critical upstream drainage area and the gradient of channel head, both of which are used to calculate the normalized channel steepness at the channel head. We then apply the new method to an active rift shoulder (Wutai Shan), and a tectonically

https://doi.org/10.5194/egusphere-2023-1428
Preprint. Discussion started: 11 August 2023

stable area (a mountain range in the Loess Plateau) in North China, to illustrate the calculation of drainage-divide migration rates. The northward migration rates at the Wutai Shan range from 0.10 to 0.13 mm/yr. The migration rates are approximately zero at the mountain range in the Loess Plateau. This study demonstrates that the migration rate of drainage divides can be determined more accurately once the cross-divide differences in uplift rate are taken into account.

Keywords

Drainage divide; Migration rate; High-resolution topographic data; DEM; Channel head

1. Introduction

The evolution of the Earth's surface is jointly controlled by tectonics, lithology, and climatic conditions (e.g., Molnar and England, 1990; Whipple, 2009; Bonnet, 2009; Gallen, 2018; Zondervan et al., 2020; Bernard et al., 2021). This provides a basis for reconstructing the past tectonic (Pritchard et al., 2009; Kirby et al., 2012; He et al., 2021; Shi et al., 2021; Schildgen et al., 2022) or climatic processes (Tucker et al., 1997; Hancock et al., 2002) through topography. The evolution of topography is fundamentally coupled with changes in drainage systems, including river's vertical and lateral movements (Whipple, 2001; Willett et al., 2014; Zeng and Tan, 2023). Previous studies have extensively investigated how river channel profiles respond to tectonic uplift (Whipple, 2001; Crosby and Whipple, 2006; Pritchard et al., 2009;

https://doi.org/10.5194/egusphere-2023-1428
Preprint. Discussion started: 11 August 2023

Kirby et al., 2012; Goren et al., 2014), lithological difference (Duvall et al., 2004; Safran et al., 2005; Forte et al., 2016), and precipitation perturbations (Schlunegger et al., 2011; Bookhagen and Strecker, 2012). However, recent studies show that widespread lateral movement of rivers (Clark et al., 2004; Deng et al., 2020; Zhao et al., 2021; Zhou et al., 2022a) also interact with the adjustment of channel profiles (Willett et al., 2014). Drainage-divide migration, therefore, may not only carry information on geologic and/or climatic disturbance (Yang et al., 2019; Su et al., 2020; He et al., 2021; Shi et al., 2021; Zeng and Tan, 2023) but also impact the extraction of tectonic information from channel profiles (Goren et al., 2014; Ma et al., 2020; Jiao et al., 2021). For this reason, the stability of drainage divides has drawn more and more attention in recent years (e.g., Authemayou et al., 2018; Vacherat et al., 2018; Chen et al., 2021; Shelef and Goren, 2021; Sakashita and Endo, 2023).

Drainage-divide migration is essentially controlled by the cross-divide difference in erosion (Beeson et al., 2017; Dahlquist et al., 2018; Chen et al., 2021; Zhou et al., 2022a). The erosion rates are routinely derived from geochronological techniques, such as cosmogenic nuclides (e.g., ^{10}Be) concentration measurements (Mandal et al., 2015; Struth et al., 2017; Sassolas-Serrayet et al., 2019), which can be used to calculate the migration velocities of drainage divides (Beeson et al., 2017; Godard et al., 2019; Hu et al., 2021). However, these techniques are usually based on samples collected from an outlet that is several kilometers away from the drainage divide and thus may not represent the erosion rates close to the drainage divide (Sassolas-Serrayet et al., 2019). Besides, the high cost of sample testing makes it very

https://doi.org/10.5194/egusphere-2023-1428
Preprint. Discussion started: 11 August 2023

challenging to determine the drainage divide's motion by measuring the erosion rates throughout the entire landscape. Hence, it would be ideal to find an accessible and efficient method that can be applied to the entire landscape and cross-checked to make full use of the ^{10}Be-derived erosion rates.

The advancement of remote sensing technology has promoted the development of geomorphic analysis theory, making it possible to determine the drainage divide's motion through topography analysis. For example, Willett et al. (2014) developed the χ method to map the dynamic state of river basins. Forte and Whipple (2018) proposed the cross-divide comparison of "Gilbert metrics" (including channel heads' relief, slope, and elevation) to determine a drainage divide's motion. Others adopted the comparison of slope angle or relief of the hillslopes across a drainage divide to deduce its stability (Scherler and Schwanghart, 2020; Ye et al., 2022). Although these geomorphic techniques are quantitative, so far, they could only determine the migration direction of drainage divides. No rates have been obtained. Braun (2018) raised a method that considers both alluvial and fluvial areas to calculate the migration velocity of an escarpment (also a drainage divide). Zhou et al. (2022a) developed a technique to calculate the migration rate through the cross-divide χ ratio of high base-level channel segments. However, the channel-head parameter such as the critical upstream area is an empirical value from previous studies, which may not be applicable in specific natural areas and, therefore, could create great uncertainties in the result of migration rates.

In this study, we choose a tectonically active area, i.e., the Wutai Shan in the

https://doi.org/10.5194/egusphere-2023-1428
Preprint. Discussion started: 11 August 2023

Shanxi rift system, and a tectonically inactive area, i.e., an unnamed mountain range in the Loess plateau, to demonstrate how to quantify drainage-divide migration rates. We use the aerial photography acquired by unmanned aerial vehicles (UAVs) and the Structure from Motion (SfM) technology to obtain the high-resolution topography data of these two areas. Based on the high-resolution data, we first identify the position of the channel heads and extract their geomorphic parameters. We then calculate the migration rates of the drainage divides using the channel-head parameters. Moreover, we improve the method in Zhou et al (2022a) to adapt it to areas where the elevations of outlets and channel heads are different across the drainage divide. We apply these two methods in each case to calculate the drainage-divide migration rates. This study aims to establish an approach to derive the migration rate of drainage divides, at a high precision and low cost, based on topographic analysis. Moreover, benefiting from the detailed tectonic research and the high-resolution topographic data on the Wutai Shan, we attempt to quantify the influence of the cross-divide difference in uplift rate on the drainage-divide migration rate.

2. Methods

2.1 Channel-head method

According to the detachment-limited stream power model (Howard and Kerby, 1983; Howard, 1994), the channel's erosion rate (E) can be expressed as:

https://doi.org/10.5194/egusphere-2023-1428
Preprint. Discussion started: 11 August 2023

$$E = KA^m S^n \quad (1)$$

where K is the erosion coefficient, A is the upstream drainage area, S is the gradient of the river channel, and m and n are empirical constants. Because of the mechanisms such as erosion threshold (Howard and Kerby, 1983; Perron et al., 2008) or landslide threshold (Burbank et al., 1996; Tucker et al., 1998), river channels (following Eq. 1) emerge at a certain distance from the drainage divide. The region between the channel head and the drainage divide is referred to as the hillslope area, where the erosion is controlled by landslide, collapse, and diffusion processes (Stoke and Dietrich, 2006; Stark, 2010; Braun et al., 2018; Dahlquist et al., 2018). The channel-head point is the highest and the closest point to the drainage divide on a river channel (Clubb et al., 2014). Therefore, the erosion rate at channel-head points (E_{ch}) can be described as:

$$E_{ch} = KA_{cr}^m S_{ch}^n \quad (2)$$

where E_{ch} is the erosion rate at channel-head points, A_{cr} is the critical upstream drainage area of a channel-head point (Duvall et al., 2004; Wobus et al., 2006), and S_{ch} is the channel-head gradient measured along the channel at the channel-head point.

To investigate the influence of the key parameters on the channel-head erosion rate, we plot the curves of the channel-head erosion rate against the critical area based on Eq. 2 for varying channel-head gradient and erosion coefficient (Fig. 1). The plots show that the channel-head erosion rate (E_{ch}) increases monotonically with the critical area (A_{cr}). When the critical area is invariant, the channel-head erosion rate also increases with the channel-head gradient. A large erosion coefficient also creates a high channel-head erosion rate. The results indicate that the side with a higher A_{cr} or

https://doi.org/10.5194/egusphere-2023-1428
Preprint. Discussion started: 11 August 2023

S_{ch} can have a higher erosion rate than the other side of the drainage divide and is more likely to pirate the opposite drainage basin. Besides, high erosion coefficient can amplify the drainage basins' erosion rate.

The drainage-divide migration is essentially controlled by the cross-divide difference in erosion rates (Beeson et al., 2017; Dahlquist et al., 2018; Chen et al., 2021). Furthermore, when one uses the cross-divide erosion rates at the channel heads to calculate the erosion difference across the divide, one should also consider the influence of differential uplift rates in these channel heads (Zhou et al., 2022a), especially in the case of tectonic tilting uplift. The drainage-divide migration rate (D_{mr}) can be obtained according to the cross-divide difference in erosion rate and uplift rate (Zhou et al., 2022a):

$$D_{mr} = \frac{\Delta E_{ch} - \Delta U_{ch}}{tan\alpha + tan\beta} \quad (3)$$

where ΔE_{ch} is the erosion rate difference between the two sides (annotated as α and β) of the drainage divide ($\Delta E_{ch} = E_{ch\alpha} - E_{ch\beta}$), ΔU_{ch} is the cross-divide difference in rock uplift rate ($\Delta U_{ch} = U_{ch\alpha} - U_{ch\beta}$), and tanα and tanβ are the gradients on both sides of the drainage divide. Combining Eqs. 2 and 3, one can derive the equation of migration velocity of drainage divides according to the parameters at the channel-head points:

$$D_{mr} = \frac{K\left[\left(A_{cr}^{m} S_{ch}^{n}\right)_{\alpha} - \left(A_{cr}^{m} S_{ch}^{n}\right)_{\beta}\right] - \Delta U_{ch}}{tan\alpha + tan\beta} \quad (4)$$

The choice of α or β is arbitrary, and the positive direction of the migration velocity is assigned as from the α to β side whereas the negative is the opposite. In this equation, we assume the erosion coefficient is unchanged in the vicinity of a drainage divide. If the exact *K* value is unknown, the drainage divide's unilateral erosion rate can be used

https://doi.org/10.5194/egusphere-2023-1428
Preprint. Discussion started: 11 August 2023

as a substitution:

$$D_{mr} = \frac{E_{\alpha}\left[1 - \frac{(A_{cr}^{m} S_{ch}^{n})_{\beta}}{(A_{cr}^{m} S_{ch}^{n})_{\alpha}}\right] - \Delta U_{ch}}{tan\alpha + tan\beta} \tag{5}$$

or:

$$D_{mr} = \frac{E_{\beta}\left[\frac{(A_{cr}^{m} S_{ch}^{n})_{\alpha}}{(A_{cr}^{m} S_{ch}^{n})_{\beta}} - 1\right] - \Delta U_{ch}}{tan\alpha + tan\beta} \tag{6}$$

E_{α} and E_{β} are the erosion rates of the α to β side of drainage divide, respectively, which can be derived through the cosmogenic nuclides (^{10}Be) concentration measurements. The regional average erosion rate ($\bar{E}$) can also be used to calculate the migration rate:

$$D_{mr} = \frac{2\bar{E}\left[\frac{(A_{cr}^{m} S_{ch}^{n})_{\alpha} - (A_{cr}^{m} S_{ch}^{n})_{\beta}}{(A_{cr}^{m} S_{ch}^{n})_{\alpha} + (A_{cr}^{m} S_{ch}^{n})_{\beta}}\right] - \Delta U_{ch}}{tan\alpha + tan\beta} \tag{7}$$

Based on Eqs. 4-7, the migration velocity of drainage divides can be estimated using channel-head parameters combined with one of the erosion-related parameters (erosion coefficient, erosion rate at one side of a drainage divide, or regional average erosion rate).

https://doi.org/10.5194/egusphere-2023-1428
Preprint. Discussion started: 11 August 2023

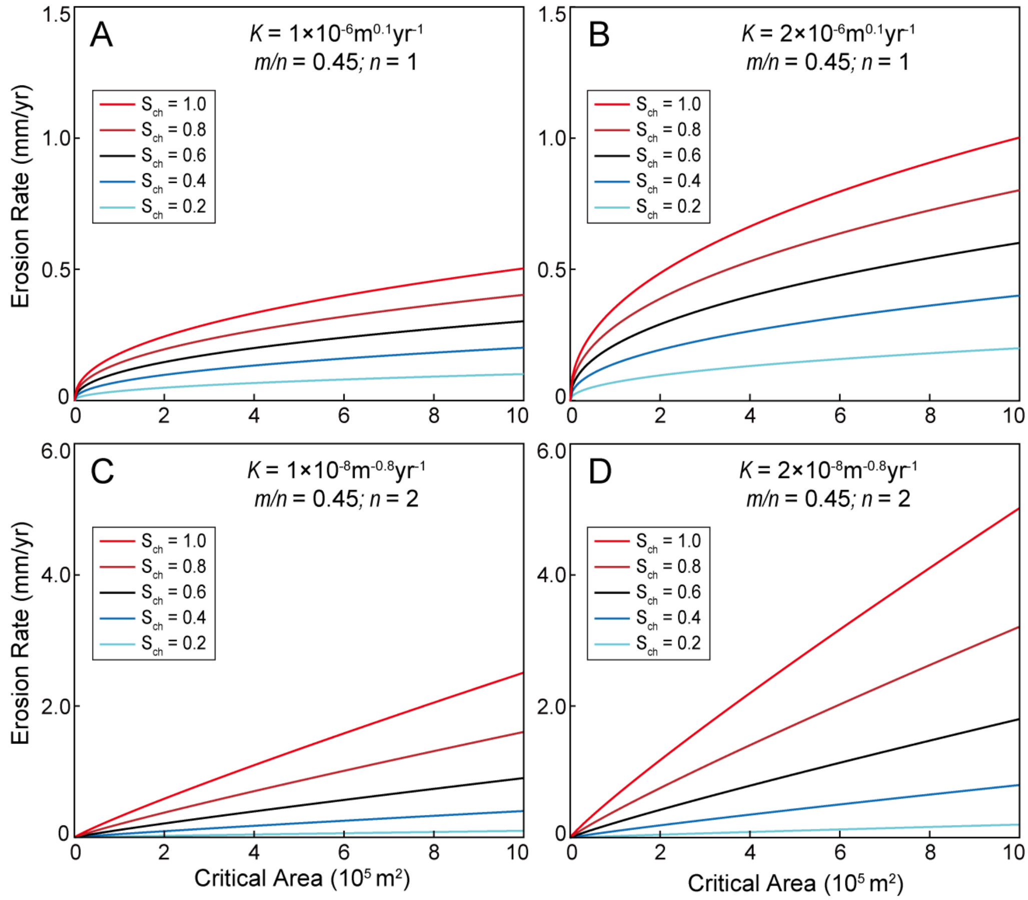

Figure 1. Curves of the channel-head erosion rate (E_{ch}) against the critical area (A_{cr}) under different values of channel-head gradient (S_{ch}) and erosion coefficient (K). We assume m = 0.45 and n = 1 in (A) and (B), and m = 0.9 and n = 2 in (C) and (D).

2.2 Channel-head-segment method

Zhou et al. (2022a) developed a method based on the cross-divide χ contrast of channel-head segments to calculate the migration velocity of drainage divides. The essence of the method is the cross-divide comparison of the channel-head segments'

https://doi.org/10.5194/egusphere-2023-1428
Preprint. Discussion started: 11 August 2023

steepness (k_{sn}) values. k_{sn} is a widely used index (Whipple et al., 1999; Wobus et al., 2006; Hilley and Arrowsmith, 2008; Kirby and Whipple, 2012) that is quantitatively related to erosion rate and erosion coefficient. Zhou et al. (2022a) proposed a cross-divide contrast of χ values, on behalf of the inverse of k_{sn}, which requires the same elevation of the channel heads and outlets across the drainage divide. Here, we release this restriction and make this method more applicable. When the regional erosion coefficient (K) is known and unchanged in the vicinity of the drainage divide, the drainage-divide migration rate can be estimated by the following equation:

$$D_{mr} = \frac{K\left[k_{sn(\alpha)}{}^{n} - k_{sn(\beta)}{}^{n}\right] - \Delta U_{ch}}{tan\alpha + tan\beta} = \frac{K\left\{\left[\frac{(z_{ch}-z_b)_\alpha}{\chi_\alpha}\right]^n - \left[\frac{(z_{ch}-z_b)_\beta}{\chi_\beta}\right]^n\right\} - \Delta U_{ch}}{tan\alpha + tan\beta} \quad (8)$$

where z_{ch} and z_b are the elevations of the channel heads and outlets, and χ is an integral function of channels' upstream area (A) to horizontal distance (x) (Perron and Royden, 2013; Willet et al., 2014). The drainage divide's unilateral erosion rate (E_α or E_β) can also be used as a substitution for the K value:

$$D_{mr} = \frac{E_\alpha\left\{1 - \left(\frac{\chi_\alpha}{\chi_\beta}\right)^n \left[\frac{(z_{ch}-z_b)_\alpha}{(z_{ch}-z_b)_\beta}\right]^{-n}\right\} - \Delta U_{ch}}{tan\alpha + tan\beta} \quad (9)$$

or:

$$D_{mr} = \frac{E_\beta\left\{\left(\frac{\chi_\alpha}{\chi_\beta}\right)^{-n} \left[\frac{(z_{ch}-z_b)_\alpha}{(z_{ch}-z_b)_\beta}\right]^{n} - 1\right\} - \Delta U_{ch}}{tan\alpha + tan\beta} \quad (10)$$

Alternatively, one can use the regional average erosion rate ($\bar{E}$) to calculate the migration rate:

$$D_{mr} = \frac{2\bar{E}\left\{\frac{\left[\frac{(z_{ch}-z_b)_\alpha}{(z_{ch}-z_b)_\beta}\right]^n - \left(\frac{\chi_\alpha}{\chi_\beta}\right)^n}{\left[\frac{(z_{ch}-z_b)_\alpha}{(z_{ch}-z_b)_\beta}\right]^n + \left(\frac{\chi_\alpha}{\chi_\beta}\right)^n}\right\} - \Delta U_{ch}}{tan\alpha + tan\beta} \quad (11)$$

Based on Eqs. 8-11, the drainage-divide migration rate can be estimated using the χ values of high-base-level channel segments combing with one of the erosion-related parameters (erosion coefficient, erosion rate at one side of a drainage divide, or regional average erosion rate).

3. Application to natural cases

We apply the new methods to two natural examples in North China, the Wutai Shan, and the Loess Plateau (Fig. 2), to demonstrate how to calculate the drainage-divide migration rates. We use UAV-acquired aerial photography and structure from motion (SfM) photogrammetry to derive the sub-meter digital elevation model of the two study areas. Based on the high-resolution topography data (sub-meter), we extract the relevant parameters and calculate the drainage-divide migration rate using the two methods above for each case. Analysis of the data is based on the Matlab toolbox TAK (Forte and Whipple, 2019) and TopoToolbox (Schwanghart and Scherler, 2014).

https://doi.org/10.5194/egusphere-2023-1428
Preprint. Discussion started: 11 August 2023

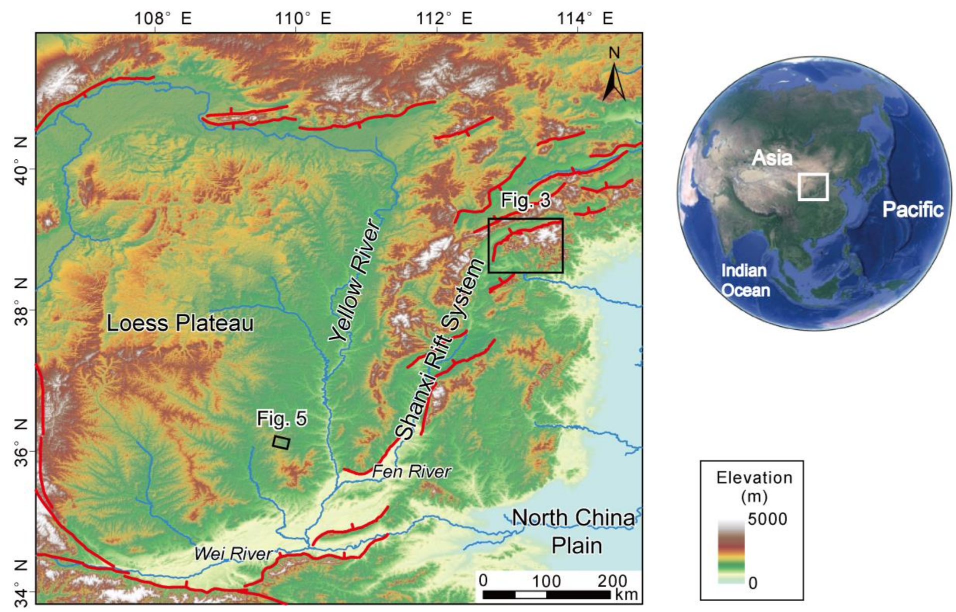

Figure 2. Locations and tectonic background of the two nature cases in North China. Red curves represent the main active faults. Black rectangles show the locations of the two nature cases.

3.1 Wutai Shan

The Wutai Shan is a tilted fault block on the shoulder of the Shanxi Rift System located in the central North China craton (Xu et al., 1993; Su et al., 2021). The tilting uplift of the Wutai Shan is controlled by the Northern Wutai Shan fault (Fig. 3A), and there is no active fault along the south edge of the Wutai Shan horst. The bedrock of the Wutai Shan area is mainly metamorphic and igneous basement rocks (Clinkscales et al., 2020; Zhou et al 2022a) and there is no obvious variation in rock erodibility and precipitation in this area.

https://doi.org/10.5194/egusphere-2023-1428
Preprint. Discussion started: 11 August 2023

To derive the erosion coefficient of the Wutai Shan area, we calculate the channel steepness values of this region and use the Kriging interpolation technique to generate the k_{sn} distribution map (Fig. 3B). According to a low-temperature thermochronology study of the Wutai Shan (Clinkscales et al., 2020), the erosion rate of the sampling area (in the footwall block of the northern boundary fault of the Wutai Shan) is about 0.25 mm/yr in the late Cenozoic. The average k_{sn} value of this area is ~80 $m^{0.9}$ (Fig. 3). According to the approach of previous studies (Kirby and Whipple, 2001; Kirkpatrick et al., 2020; Ma et al., 2020), the erosion coefficient is ~3×10^{-6} $m^{0.1}yr^{-1}$ in the Wutai Shan area.

We then apply the two above methods in this area to calculate the migration velocity of the drainage divide in the Wutai Shan. We first randomly choose three pairs of rivers (Fig. 4A) and make their slope-area plots (Figs. 4B, E, H) and the χ-plots (Figs. 4C, F, I). According to the breaking point of the slope-area plot (Duvall et al., 2004) and its corresponding position on the χ-plot, we can separate hillslope and channel areas and mark the position of the channel heads on the plots and the topography map (Fig. 4A). For the slope-area plots, we derive the value of critical upstream drainage area (A_{cr}) according to the position of the channel heads. Because the slopes of the channel-head points varies, we use the average slope of the hillslope area as the value of channel-head gradient (S_{ch}). Moreover, for the χ-plots (Figs. 4C, F, I), we obtain the elevations of outlets (z_b) and channel heads (z_{ch}) of the channel segment, and the χ value according to the position of the channel-head points.

If we assume the rock uplift rate decreases linearly from 0.25 to 0 mm/yr from

https://doi.org/10.5194/egusphere-2023-1428
Preprint. Discussion started: 11 August 2023

northwest to southeast of the Wutai Shan horst (~40 km wide), the cross-divide uplift difference in the channel-head points (ΔU_{ch}) (the distance along the normal direction of the boundary fault is ~600 m) is ~0.004 mm/yr. The tanα and tanβ are in line with the gradient of channel-head points (S_{ch}) on each side of the drainage divide (Figs. 4D, G, J). We assume n = 1 and m = 0.45 in the calculation following previous studies (Wobus et al., 2006; DiBiase et al., 2010; Perron and Royden, 2013; Wang et al., 2021). After determining these parameters, we adopt the channel-head (Eq. 4) and channel-head-segment (Eq. 8) methods to calculate the migration rates. The required data for calculation and the migration rates are shown in Table 1.

Both the slope-area plots (Figs. 4B, E, H) and the χ-plots (Figs. 4C, F, I) show that distinct character of the rivers across the drainage divide. For the first site (Fig. 4D), the migration rates calculated by both the channel-head and channel-head-segment methods are 0.12 mm/yr (northward). For the second site (Fig. 4G), the migration rates derived from the two methods are 0.11 mm/yr and 0.13 mm/yr (northward), respectively. For the third site (Fig. 4J), the migration rates are 0.12 mm/yr and 0.10 mm/yr (northward), respectively. The drainage divides of all three points are predicted to migrate northward, which is consistent with previous result inferred by the cross-divide contrast of slopes (Zhou et al., 2022b). Furthermore, the migration velocities calculated by the two methods are comparable in all three sites.

https://doi.org/10.5194/egusphere-2023-1428
Preprint. Discussion started: 11 August 2023

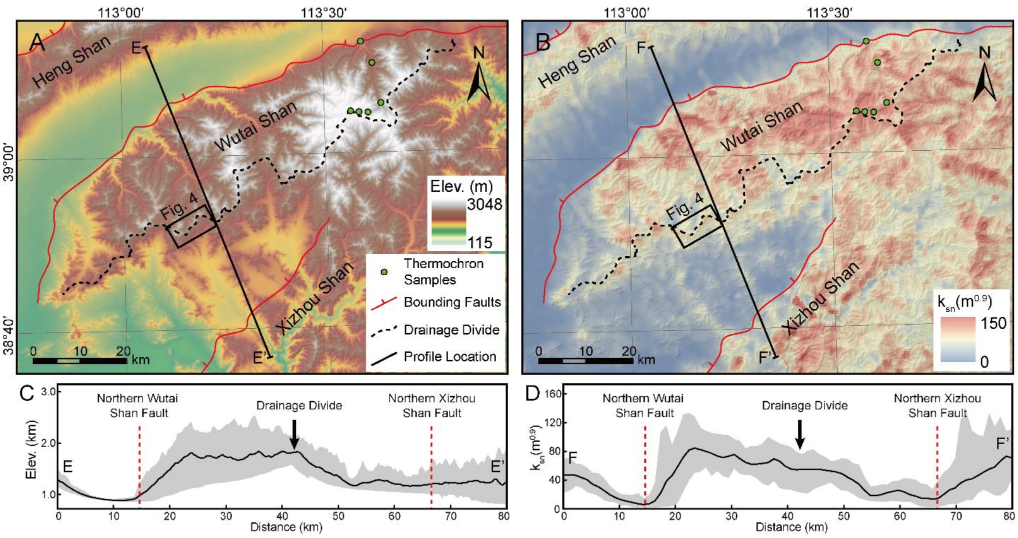

Figure 3. (**A & B**) Topography and normalized channel steepness (k_{sn}) distribution of the Wutai Shan horst and surrounding area. The black dashed curve shows the location of the main drainage divide. Red curves show the main bounding faults. The black straight lines show the location of the profiles E-E' and F-F'. Black rectangles show the area of aerial photography (Fig. 4A). Green dots denote the locations of the low-temperature thermochronology samples in Clinkscales et al. (2020). The topography data (ALOS DEM, 12.5 m resolution) is downloaded from the Alaska Satellite Facility (ASF) Data Search (https://search.asf.alaska.edu/). The k_{sn} is calculated using TopoToolbox (Schwanghart and Scherler, 2014) based on Matlab, and the interpolation uses the Kriging method. (**C**) The topography swath profile along E-E' in Fig. 3A. (**D**) The k_{sn} swath profile along F-F' in Fig. 3B. The red dotted line shows the location of the main bounding faults and the black arrow shows the location of the main drainage divide. Both swath profiles are 20 km wide (10 km on each side).

https://doi.org/10.5194/egusphere-2023-1428
Preprint. Discussion started: 11 August 2023

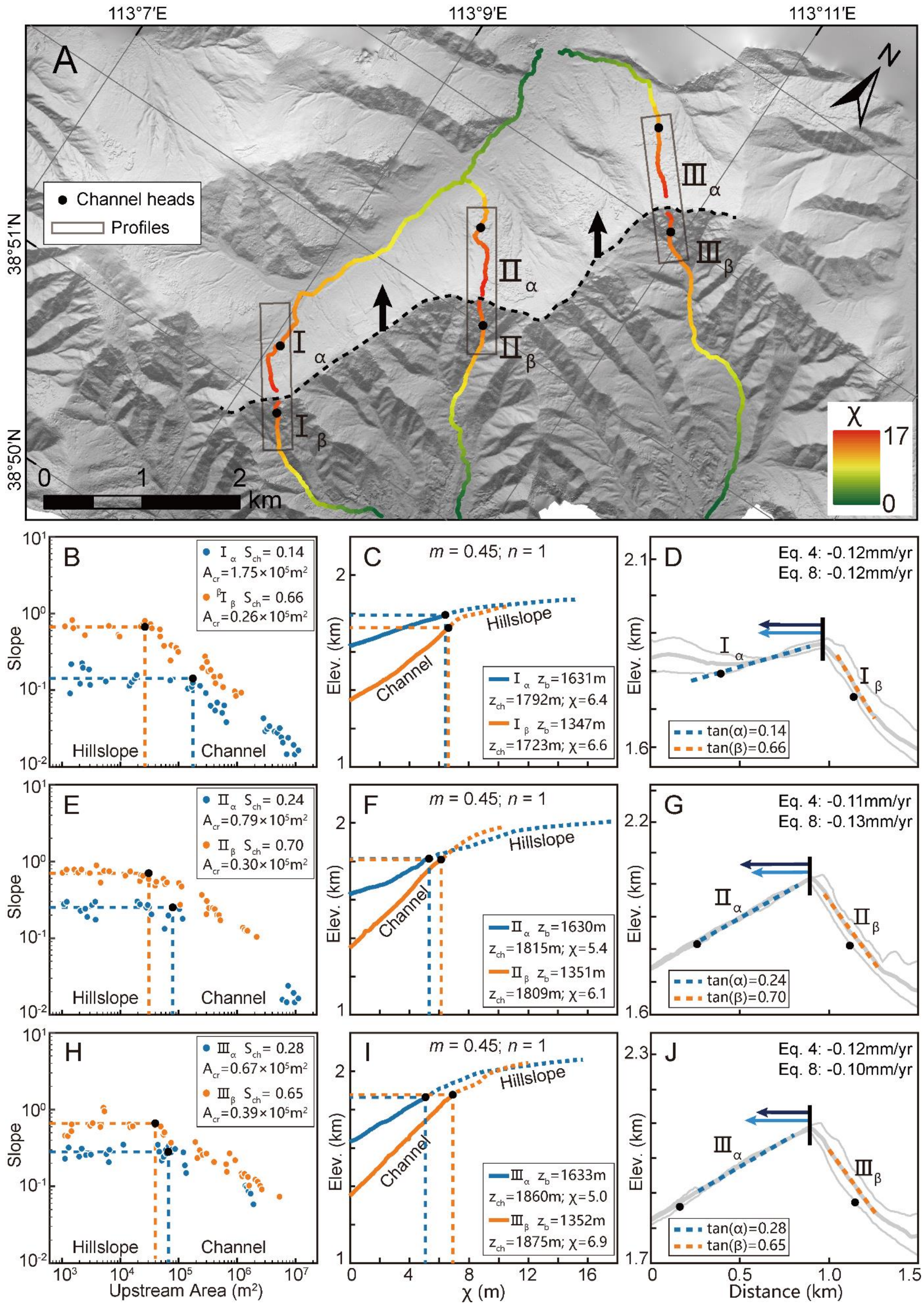

Figure 4. Analytical results of the Wutai Shan. (**A**) High-resolution topographic map (sub-meter) of the Wutai Shan. The black dashed curve shows the location of the main drainage divide. Colored curves show the three pairs of selected channels used for analysis. The black dots are the channel heads. Black rectangles show the location of the cross-divide topography swath profiles. The black arrows show the direction of drainage-divide migration (**B, E, H**) Slope-area plots of the three pairs of selected channels. The blue and orange dots are the slope-area plots of the north (α) and south (β) sides of the drainage divide respectively. The black dots represent the channel heads. (**C, F, I**) χ-plots of the selected channels. The blue and orange curves are the χ-plots of the north (α) and south (β) sides of the drainage divide respectively. The black dots represent the channel heads. (**D, G, J**) Cross-divide topography swath profiles with the drainage-divide migration rates. The locations of the profiles are in Fig. 4A. The light and dark blue arrows are the drainage-divide migration rates calculated by the channel-head (Eq. 4) and channel-head-segment (Eq. 8) method respectively.

3.2 An unnamed mountain range in the Loess Plateau

The Loess Plateau is hosted by the tectonically stable Ordos Block of the North China craton (Yin, 2010 Su et al., 2021). It accumulates tens to hundreds of meters of eolian sediments over the past 2.6 million years (Yan et al., 2014), draping preexisting topography (Xiong et al., 2014). There is no active fault within the study area. The lithology of the study site is mainly loess; there is little to no variation in rock

https://doi.org/10.5194/egusphere-2023-1428
Preprint. Discussion started: 11 August 2023

erodibility and precipitation within the area (Shi et al., 2020; Zhou et al., 2022b).

We apply the two methods in this area to calculate the drainage-divide migration rate. Similar to the Wutai Shan case, we first randomly choose three pairs of rivers and make their slope-area plots (Figs. 5 B, E, H) and the χ-plots (Figs. 5 C, F, I). Then we mark the position of the channel-head points on the topography map (Fig. 5A), slope-area plots, and χ-plots. According to its position, we derive the A_{cr} values from the slope-area plots (Figs. 5 B, E, H) and the χ values and the elevations of channel-head segments' outlets (z_b) and heads (z_{ch}) from the χ-plots (Figs. 5 C, F, I). We also acquire the average slope of the hillslope area and derive the S_{ch}, tanα, and tanβ values.

The rate of soil erosion in the study area is about 500 $t{\cdot}km^{-2}yr^{-1}$ (Fu, 1989). If we assume the density of Loess is 1.65 $t{\cdot}m^{-3}$, the average erosion rate here is about 0.3 $mm{\cdot}yr^{-1}$. Because there is no obvious unequal uplift in this region, we assume that ΔU_{ch} is zero. We also assume $n = 1$ and $m = 0.45$ in the calculation. Then, we use the methods of channel-head parameters (Eq. 7) and channel segments (Eq. 11) to calculate the drainage-divide migration rates. The required data for calculation and the migration rates are shown in Table 1.

All results of the three points show that the drainage-divide migration rate here is close to zero, no matter which method is used in the calculation. The results show that the drainage divide of the study site is in topographical equilibrium, which is consistent with the inference in previous studies (Willett et al., 2014, Zhou et al., 2022b).

https://doi.org/10.5194/egusphere-2023-1428
Preprint. Discussion started: 11 August 2023

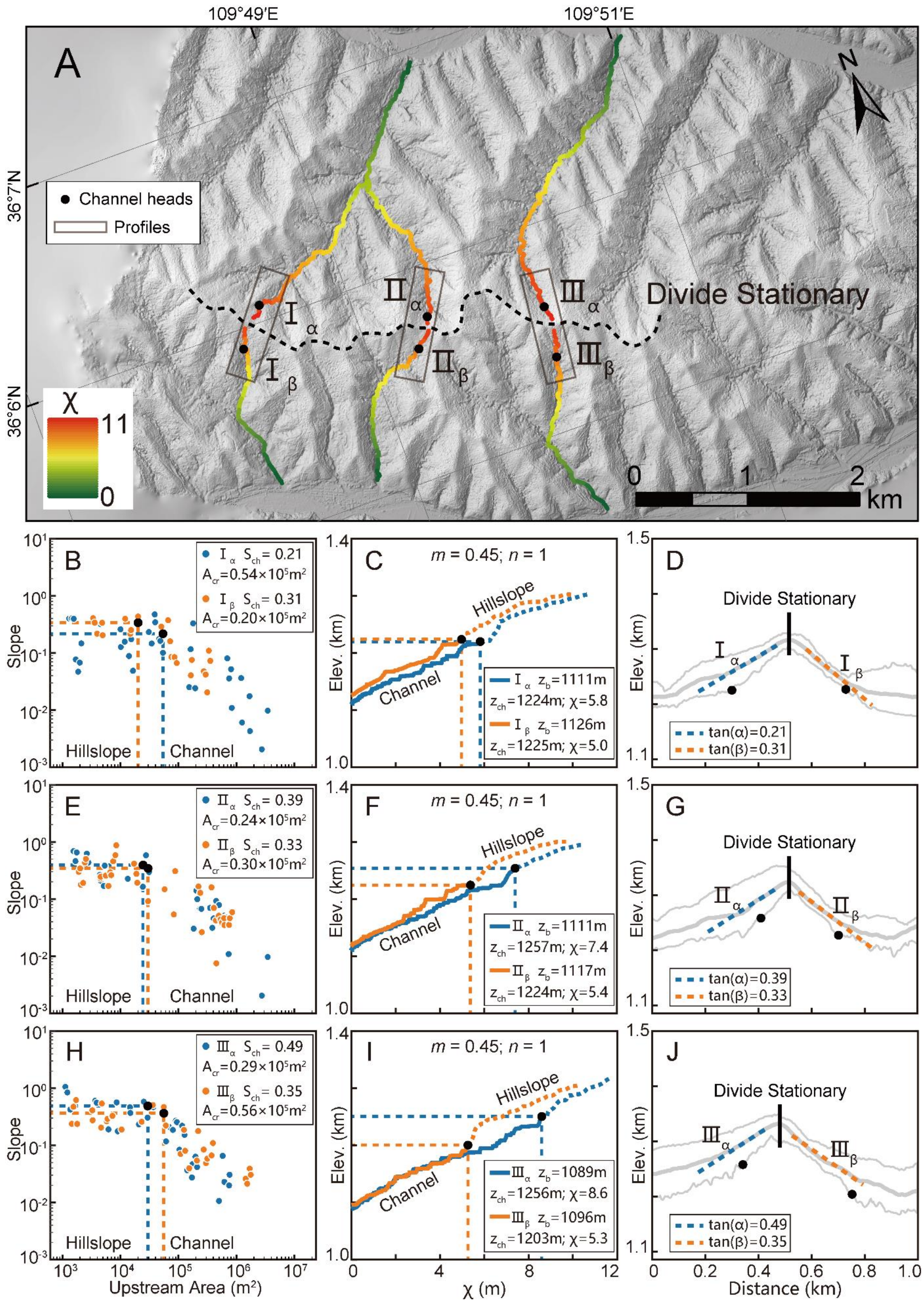

https://doi.org/10.5194/egusphere-2023-1428
Preprint. Discussion started: 11 August 2023

Figure 5. Analytical results of a mountain range in the Loess Plateau. (**A**) High-resolution topographic map (sub-meter). The black dotted curve shows the location of the main drainage divide. Colored curves show the three pairs of selected channels used for analysis. The black dots represent the channel heads. Black rectangles show the location of the cross-divide topography swath profiles. (**B, E, H**) Slope-area plots of the three pairs of selected channels. The blue and orange dots are the data of the north (α) and south (β) sides of the drainage divide respectively. The black dots represent the channel heads. (**C, F, I**) χ-plots of the selected channels. The blue and orange curves are the χ-plots of the north (α) and south (β) sides of the drainage divide respectively. The black dots represent the channel heads. (**D, G, J**) The cross-divide topography swath profiles. The locations of the swath profiles are in Panel A.

Table 1. Channel's parameters and the migration rates of the drainage divides of the two natural cases.

	No.	A_{cr} ($\times 10^5 m^2$)	S_{ch}	z_b (m)	z_{ch} (m)	χ	tanα	tanβ	ΔU_{ch} (mm/yr)	D_{mr} (mm/yr) (Channel-head method)	D_{mr} (mm/yr) (Channel-head-segment method)
Wutai Shan	Fig. 4 I_{α}	1.75	0.14	1631	1792	6.4	0.14	0.66	~0.004	-0.12	-0.12
	Fig. 4 I_{β}	0.26	0.66	1347	1723	6.6					
	Fig. 4 II_{α}	0.79	0.24	1630	1815	5.4	0.24	0.70	~0.004	-0.11	-0.13
	Fig. 4 II_{β}	0.30	0.70	1351	1809	6.1					
	Fig. 4 III_{α}	0.67	0.28	1633	1860	5.0	0.28	0.65	~0.004	-0.12	-0.10
	Fig. 4 III_{β}	0.39	0.65	1352	1875	6.9					
Loess Plateau	Fig. 5 I_{α}	0.54	0.21	1111	1224	5.8	0.21	0.31	0	0.02	-0.01
	Fig. 5 I_{β}	0.20	0.31	1126	1225	5.0					
	Fig. 5 II_{α}	0.24	0.39	1111	1257	7.4	0.39	0.33	0	0.03	-0.01
	Fig. 5 II_{β}	0.30	0.33	1117	1224	5.4					
	Fig. 5 III_{α}	0.29	0.49	1089	1256	8.6	0.49	0.35	0	0.01	-0.01
	Fig. 5 III_{β}	0.56	0.35	1096	1203	5.3					

https://doi.org/10.5194/egusphere-2023-1428
Preprint. Discussion started: 11 August 2023

4. Discussion

4.1 Location of channel heads

Willett et al. (2014) pioneered the use of cross-divide χ contrast to gauge the horizontal motion of drainage divides. According to their method, drainage divides are predicted to move toward the side with a higher χ value to achieve geomorphic equilibrium. However, in a region with spatially variable uplift rates, lithology, or precipitation, χ contrast may fail to reflect the drainage-divide migration (Willett et al., 2014; Whipple et al., 2017; Forte and Whipple, 2018; Zhou and Tan, 2023). In the tectonically active area, the cross-divide χ contrast can only be used in a small area where rock type, precipitation, and uplift rate are nearly uniform (Willett et al., 2014). Forte and Whipple (2018) proposed the Gilbert metrics to measure the stability of drainage divides. Zhou et al. (2022a) combined the advantages of the χ and Gilbert metrics methods, proposed to use the χ contrast with a high base level to calculate the k_{sn} values at the channel heads on both sides of a drainage divide, and quantified the migration rate of drainage divides at the eastern margin of Tibet.

To reduce the cross-divide difference in uplift rate, precipitation, and rock strength, these methods should compare the parameters of points (slope, relief, elevation, and k_{sn}) on both sides of the divide as closely as possible. As the hillslope area (above the channel head) does not follow Eq. 1 (Stoke and Dietrich, 2006; Stark, 2010; Braun et al., 2018; Dahlquist et al., 2018)), the channel heads are the closest point to the divide, following Eq. 1. Channel heads, therefore, are suitable for

https://doi.org/10.5194/egusphere-2023-1428
Preprint. Discussion started: 11 August 2023

measuring the drainage-divide stability with the parameters of the upstream drainage area and channel gradient (Forte and Whipple, 2018; Zhou et al., 2022a; this study). However, the location of the channel heads is usually based on empirical parameters, which may introduce errors in the result of drainage-divide stability. In this study, we advocate the use of high-resolution DEM to determine a more accurate position and related parameters of the channel head, given that the use of UAVs to obtain the local DEM has become highly efficient. We advance the theory to calculate the drainage-divide migration rate based on the measured channel-head parameters. With the help of the aerial photography of UAVs and the SfM techniques, one can obtain the sub-meter resolution topography data of drainage divides (Figs. 4A & 5A) and get the required parameters (including the exact locations of the channel heads across the drainage divide) through topography analysis, which could improve the quantitative research on the drainage-divide migration. Furthermore, the method provides a new avenue to combine with catchment-wide ^{10}Be erosion rate or low-temperature thermochronology data to calculate the migration rate, which has great potentials of application in places where some variables are hard to be constrained.

4.2 Cross-divide difference in uplift rate of the channel heads

Although the channel heads across the divide are very close on the spatial scale of an orogenic belt, differential uplift between the channel heads (ΔU_{ch}) could still exist, especially in a tilting horst, such as the Wutai Shan. The cross-divide difference in

https://doi.org/10.5194/egusphere-2023-1428
Preprint. Discussion started: 11 August 2023

uplift rate could impact the calculation of the migration rate of drainage divides (Zhou et al., 2022a). Although the differential uplift rate is usually small enough to be ignored in some natural cases, its influence on the migration rate of drainage divides should be taken into account theoretically (Zhou et al., 2022a).

In this study, we quantify the influence of cross-divide difference in rock uplift rate (ΔU_{ch}) on the calculation of the migration rate of drainage divides at the Wutai Shan, benefiting from the available tectonic and chronological research (Clinkscales et al., 2020) and the newly obtained high-resolution topographic data. In the Wutai Shan horst, ΔU_{ch} across the drainage divide is ~0.004 mm/yr. We estimated the influence of ΔU_{ch} on the drainage-divide migration rate in the case study of the Wutai Shan, which can reduce the error theoretically. If ΔU_{ch} is ignored, the drainage-divide migration rate would decrease by ~4% in the Wutai Shan case. Although ~4% seems to be negligible, such a ratio will increase if the mountain belt is narrower, the tilting uplift is stronger, or the divide is closer to the steady state (i.e., the migration rate is lower). In other words, the differential uplift may play a significant influence on the measurement of drainage-divide stability in some situations. Consider an extreme example: when the main drainage divide of a tilting mountain range (relatively narrow in width) is at a steady state, the gradient, relief, and elevation of the channel heads (collectively called "Gilbert metrics" (Forte and Whipple, 2018)) will show a systematic cross-divide difference in theory. In this case, the drainage divide would be considered unstable if ΔU_{ch} were neglected. Therefore, ΔU_{ch} should be taken into account, either in a qualitative or a quantitative evaluation of the stability of drainage

https://doi.org/10.5194/egusphere-2023-1428
Preprint. Discussion started: 11 August 2023

divides using the parameters on the channel heads.

5. Conclusions

We have developed a new method to calculate the migration rate of drainage divides based upon channel-head parameters. We have also improved the channel-head-segment method in the previous study (Zhou et al., 2022a) to adapt the theory to areas where the elevations of outlets and channel heads are different across the drainage divide.

Using the high-resolution topographic data, we determined the exact locations of the channel heads on both sides of the drainage divide and quantified the drainage-divide migration rates in two natural cases (the Wutai Shan in the Shanxi Rift System, and an unnamed mountain range in the Loess Plateau). The migration rates of the study sites in the Wutai Shan are 0.10-0.13 mm/yr (moving north). The rates are close to zero in the Loess Plateau.

Based on the locations of the channel heads and the uplift gradient of the mountain, we calculated the cross-divide difference in uplift rate at the channel heads (ΔU_{ch}), which is taken into account in the calculation of the drainage-divide migration rate for the first time. If ΔU_{ch} is overlooked, the drainage-divide migration rate would be underestimated. We suggest that ΔU_{ch} should be considered if one aims to assess the stability of drainage divides based on the cross-divide difference in channel-head parameters.

https://doi.org/10.5194/egusphere-2023-1428
Preprint. Discussion started: 11 August 2023

Data availability. The analysis of data is based on the Matlab toolbox TAK (Forte and Whipple, 2019) and TopoToolbox (Schwanghart and Scherler, 2014). The topography data (ALOS DEM, 12.5 m resolution) is downloaded from the Alaska Satellite Facility (ASF) Data Search (https://search.asf.alaska.edu/).

Financial support. This study is supported by the CAS Pioneer Hundred Talents Program (E2K2010010) and the Fundamental Research Funds for the State Key Laboratory of Earthquake Dynamics (LED2021A02).

Competing interests. The authors declare that they have no conflict of interest.

Author contributions. XT and CZ contributed to the design of research scheme. CZ performed the geomorphic analyses. CZ, XT, and FS carried out field data collection. CZ, XT, YL, and FS contributed to the text and reviewed the paper.

References

Authemayou, C., Brocard, G., Delcaillau, B., Molliex, S., Pedoja, K., Husson, L., et al., 2018. Unraveling the roles of asymmetric uplift, normal faulting and groundwater flow to drainage rearrangement in an emerging karstic landscape. Earth Surface Processes and Landforms, 43(9), 1885-1898. https://doi.org/10.1002/esp.4363

Beeson, H.W., McCoy, S.W., Keen-Zebert, A., 2017. Geometric disequilibrium of river basins produces long-lived transient landscapes. Earth Planet Sc Lett 475,

https://doi.org/10.5194/egusphere-2023-1428
Preprint. Discussion started: 11 August 2023

34-43. https://doi.org/10.1016/j.epsl.2017.07.010
Bernard, T., Sinclair, H.D., Gailleton, B., Fox, M., 2021. Formation of Longitudinal River Valleys and the Fixing of Drainage Divides in Response to Exhumation of Crystalline Basement. Geophys Res Lett 48. https://doi.org/10.1029/2020gl092210.
Bonnet, S., 2009. Shrinking and splitting of drainage basins in orogenic landscapes from the migration of the main drainage divide. Nature Geoscience 2, 766-771. https://doi.org/10.1038/ngeo666
Bookhagen, B., Strecker, M.R., 2012. Spatiotemporal trends in erosion rates across a pronounced rainfall gradient: Examples from the southern Central Andes. Earth Planet Sc Lett 327-328, 97-110. ttps://doi.org/10.1016/j.epsl.2012.02.005
Braun, J., 2018. A review of numerical modeling studies of passive margin escarpments leading to a new analytical expression for the rate of escarpment migration velocity. Gondwana Research 53, 209-224. https://doi.org/10.1016/j.gr.2017.04.012
Burbank, D.W., Leland, J., Fielding, E., Anderson, R.S., Brozovic, N., Reid, M.R., Duncan, C., 1996. Bedrock incision, rock uplift and threshold hillslopes in the northwestern Himalayas. Nature 379, 505–510. https://doi.org/10.1038/379505a0
Chen, C.-Y., Willett, S.D., Christl, M., Shyu, J.B.H., 2021. Drainage basin dynamics during the transition from early to mature orogeny in Southern Taiwan. Earth Planet Sc Lett 562. https://doi.org/10.1016/j.epsl.2021.116874
Clark, M.K., Schoenbohm, L.M., Royden, L.H., Whipple, K.X., Burchfiel, B.C.,

Zhang, X., Tang, W., Wang, E., Chen, L., 2004. Surface uplift, tectonics, and erosion of eastern Tibet from large-scale drainage patterns. Tectonics 23, 1-20. https://doi.org/10.1029/2002tc001402

Clinkscales, C., Kapp, P., Wang, H., 2020. Exhumation history of the north-central Shanxi Rift, North China, revealed by low-temperature thermochronology. Earth Planet Sc Lett 536, 116146. https://doi.org/10.1016/j.epsl.2020.116146

Clubb, F.J., Mudd, S.M., Milodowski, D.T., Hurst, M.D., Slater, L.J., 2014. Objective extraction of channel heads from high-resolution topographic data. Water Resources Research 50, 4283-4304. https://doi.org/10.1002/2013wr015167

Crosby, B.T., Whipple, K.X., 2006. Knickpoint initiation and distribution within fluvial networks: 236 waterfalls in the Waipaoa River, North Island, New Zealand. Geomorphology 82, 16-38. https://doi.org/10.1016/j.geomorph.2005.08.023

Dahlquist, M.P., West, A.J., Li, G., 2018. Landslide-driven drainage divide migration. Geology 46, 403-406. https://doi.org/10.1130/g39916.1

Deng, B., Chew, D., Mark, C., Liu, S., Cogné, N., Jiang, L., O'Sullivan, G., Li, Z., Li, J., 2020. Late Cenozoic drainage reorganization of the paleo-Yangtze river constrained by multi-proxy provenance analysis of the Paleo-lake Xigeda. GSA Bulletin. https://doi.org/10.1130/b35579.1

DiBiase, R.A., Whipple, K.X., Heimsath, A.M., Ouimet, W.B., 2010. Landscape form and millennial erosion rates in the San Gabriel Mountains, CA. Earth Planet Sc Lett 289, 134-144. https://doi.org/10.1016/j.epsl.2009.10.036

https://doi.org/10.5194/egusphere-2023-1428
Preprint. Discussion started: 11 August 2023

Duvall, A., 2004. Tectonic and lithologic controls on bedrock channel profiles and processes in coastal California. J Geophys Res 109. https://doi.org/10.1029/2003jf000086

Forte, A.M., Whipple, K.X., 2018. Criteria and tools for determining drainage divide stability. Earth Planet Sc Lett 493, 102–117. https://doi.org/10.1016/j.epsl.2018.04.026

Forte, A.M., Whipple, K.X., 2019. Short communication: The Topographic Analysis Kit (TAK) for TopoToolbox. Earth Surface Dynamics 7, 87–95. https://doi.org/10.5194/esurf-7-87-2019

Forte, A.M., Yanites, B.J., Whipple, K.X., 2016. Complexities of landscape evolution during incision through layered stratigraphy with contrasts in rock strength. Earth Surface Processes and Landforms 41, 1736-1757. https://doi.org/10.1002/esp.3947

Fu, B., 1989. Soil erosion and its control in the loess plateau of China. Soil Use and Management 5, 76-82. https://doi.org/10.1111/j.1475-2743.1989.tb00765.x

Gallen, S.F., 2018. Lithologic controls on landscape dynamics and aquatic species evolution in post-orogenic mountains. Earth Planet Sc Lett 493, 150-160. https://doi.org/10.1016/j.epsl.2018.04.029

Godard, V., Dosseto, A., Fleury, J., Bellier, O., Siame, L., 2019. Transient landscape dynamics across the Southeastern Australian Escarpment. Earth Planet Sc Lett 506, 397-406. https://doi.org/10.1016/j.epsl.2018.11.017

Goren, L., Fox, M., Willett, S.D., 2014. Tectonics from fluvial topography using

https://doi.org/10.5194/egusphere-2023-1428
Preprint. Discussion started: 11 August 2023

formal linear inversion: Theory and applications to the Inyo Mountains, California. Journal of Geophysical Research: Earth Surface 119, 1651-1681. https://doi.org/10.1002/2014jf003079

Hancock, G.S., Anderson, R.S., 2002. Numerical modeling of fluvial strath-terrace formation in response to oscillating climate. GSA Bulletin 114, 1131-1142. https://doi.org/10.1130/0016-7606(2002)114<1131:nmofst>2.0.co;2

He, C., Yang, C.J., Turowski, J.M., Rao, G., Roda-Boluda, D.C., Yuan, X.P., 2021. Constraining tectonic uplift and advection from the main drainage divide of a mountain belt. Nat Commun 12, 544. https://doi.org/10.1038/s41467-020-20748-2

Hilley, G.E., Arrowsmith, J.R., 2008. Geomorphic response to uplift along the Dragon's Back pressure ridge, Carrizo Plain, California. Geology 36. https://doi.org/10.1130/g24517a.1

Howard, A.D., Dietrich, W.E., Seidl, M.A., 1994. Modeling fluvial erosion on regional to continental scales. Journal of Geophysical Research: Solid Earth 99, 13971-13986. https://doi.org/10.1029/94jb00744

Howard, A.D., Kerby, G., 1983. Channel changes in badlands. Geological Society of America Bulletin 94, 739. https://doi.org/10.1130/0016-7606(1983)94<739:CCIB>2.0.CO;2

Hu, K., Fang, X., Ferrier, K.L., Granger, D.E., Zhao, Z., Ruetenik, G.A., 2021. Covariation of cross-divide differences in denudation rate and χ: Implications for drainage basin reorganization in the Qilian Shan, northeast Tibet. Earth Planet Sc

https://doi.org/10.5194/egusphere-2023-1428
Preprint. Discussion started: 11 August 2023

Lett 562, 116812. https://doi.org/10.1016/j.epsl.2021.116812

Jiao, R., Fox, M., Yang, R., 2022. Late Cenozoic erosion pattern of the eastern margin of the Sichuan Basin: Implications for the drainage evolution of the Yangtze River. Geomorphology 398, 108025. https://doi.org/10.1016/j.geomorph.2021.108025

Kirby, E., Whipple, K., 2001. Quantifying differential rock-uplift rates via stream profile analysis. Geology 29, 415-418. https://doi.org/10.1130/0091-7613(2001)029<0415:Qdrurv>2.0.Co;2

Kirby, E., Whipple, K.X., 2012. Expression of active tectonics in erosional landscapes. J Struct Geol 44, 54-75. https://doi.org/10.1016/j.jsg.2012.07.009

Kirkpatrick, H.M., Moon, S., Yin, A., Harrison, T.M., 2020. Impact of fault damage on eastern Tibet topography. Geology 48. https://doi.org/10.1130/g48179.1

Ma, Z., Zhang, H., Wang, Y., Tao, Y., Li, X., 2020. Inversion of Dadu River Bedrock Channels for the Late Cenozoic Uplift History of the Eastern Tibetan Plateau. Geophys Res Lett 47. https://doi.org/10.1029/2019gl086882

Mandal, S.K., Lupker, M., Burg, J.-P., Valla, P.G., Haghipour, N., Christl, M., 2015. Spatial variability of 10 Be-derived erosion rates across the southern Peninsular Indian escarpment: A key to landscape evolution across passive margins. Earth Planet Sc Lett 425, 154-167. https://doi.org/10.1016/j.epsl.2015.05.050

Molnar, P., England, P., 1990. Late Cenozoic uplift of mountain ranges and global climate change: chicken or egg? Nature 346, 29-34. https://doi.org/10.1038_346029a0

https://doi.org/10.5194/egusphere-2023-1428
Preprint. Discussion started: 11 August 2023

Perron, J.T., Dietrich, W.E., Kirchner, J.W., 2008. Controls on the spacing of first-order valleys. J Geophys Res 113. https://doi.org/10.1029/2007jf000977

Perron, J.T., Royden, L., 2013. An integral approach to bedrock river profile analysis. Earth Surface Processes and Landforms 38, 570-576. https://doi.org/10.1002/esp.3302

Pritchard, D., Roberts, G.G., White, N.J., Richardson, C.N., 2009. Uplift histories from river profiles. Geophys Res Lett 36. https://doi.org/10.1029/2009gl040928

Safran, E.B., Bierman, P.R., Aalto, R., Dunne, T., Whipple, K.X., Caffee, M., 2005. Erosion rates driven by channel network incision in the Bolivian Andes. Earth Surface Processes and Landforms 30, 1007-1024. https://doi.org/10.1002/esp.1259

Sassolas-Serrayet, T., Cattin, R., Ferry, M., Godard, V., Simoes, M., 2019. Estimating the disequilibrium in denudation rates due to divide migration at the scale of river basins. Earth Surface Dynamics 7, 1041-1057. https://doi.org/10.5194/esurf-7-1041-2019

Scherler, D., Schwanghart, W., 2020. Drainage divide networks – Part 2: Response to perturbations. Earth Surface Dynamics 8, 261-274. https://doi.org/10.5194/esurf-8-261-2020

Schildgen, T.F., van der Beek, P.A., D'Arcy, M., Roda-Boluda, D., Orr, E.N., Wittmann, H., 2022. Quantifying drainage-divide migration from orographic rainfall over geologic timescales: Sierra de Aconquija, southern Central Andes. Earth Planet Sc Lett 579, 117345. https://doi.org/10.1016/j.epsl.2021.117345

https://doi.org/10.5194/egusphere-2023-1428
Preprint. Discussion started: 11 August 2023

Schlunegger, F., Norton, K.P., Zeilinger, G., 2011. Climatic Forcing on Channel Profiles in the Eastern Cordillera of the Coroico Region, Bolivia. The Journal of Geology 119, 97-107. https://doi.org/10.1086/657407

Schwanghart, W., D., S., 2014. Short Communication: TopoToolbox 2 – MATLAB-based software for topographic analysis and modeling in Earth surface sciences. Earth Surface Dynamics 2, 1-7. https://doi.org/10.5194/esurf-2-1-2014

Shelef, E., Goren, L., 2021. The rate and extent of wind-gap migration regulated by tributary confluences and avulsions. Earth Surface Dynamics, 9(4), 687-700. https://doi.org/10.5194/esurf-9-687-2021

Shi, F., Tan, X., Zhou, C., Liu, Y., 2021. Impact of asymmetric uplift on mountain asymmetry: Analytical solution, numerical modeling, and natural examples. Geomorphology 389, 107862. https://doi.org/10.1016/j.geomorph.2021.107862

Shi, W., Dong, S., Hu, J., 2020. Neotectonics around the Ordos Block, North China: A review and new insights. Earth-Science Reviews 200, 102969. https://doi.org/10.1016/j.earscirev.2019.102969

Stark, C.P., 2010. Oscillatory motion of drainage divides. Geophys Res Lett 37. https://doi.org/10.1029/2009gl040851

Stock, J.D., Dietrich, W.E., 2006. Erosion of steepland valleys by debris flows. Geological Society of America Bulletin 118, 1125-1148. https://doi.org/10.1130/b25902.1

Struth, L., Teixell, A., Owen, L.A., Babault, J., 2017. Plateau reduction by drainage divide migration in the Eastern Cordillera of Colombia defined by morphometry

https://doi.org/10.5194/egusphere-2023-1428
Preprint. Discussion started: 11 August 2023

and ^{10}Be terrestrial cosmogenic nuclides. Earth Surface Processes and Landforms 42, 1155-1170. https://doi.org/10.1002/esp.4079

Su, P., He, H., Tan, X., Liu, Y., Shi, F., Kirby, E., 2021. Initiation and Evolution of the Shanxi Rift System in North China: Evidence From Low-Temperature Thermochronology in a Plate Reconstruction Framework. Tectonics 40. https://doi.org/10.1029/2020tc006298

Su, Q., Wang, X., Lu, H., Xie, H., 2020. Dynamic Divide Migration as a Response to Asymmetric Uplift: An Example from the Zhongtiao Shan, North China. Remote Sensing 12. https://doi.org/10.3390/rs12244188

Tucker, G.E., Bras, R.L., 1998. Hillslope processes, drainage density, and landscape morphology. Water Resources Research 34, 2751-2764. https://doi.org/10.1029/98wr01474

Tucker, G.E., Slingerland, R., 1997. Drainage basin responses to climate change. Water Resources Research 33, 2031-2047. https://doi.org/10.1029/97wr00409

Vacherat, A., Bonnet, S., Mouthereau, F., 2018. Drainage reorganization and divide migration induced by the excavation of the Ebro basin (NE Spain). Earth Surface Dynamics, 6(2), 369-387. https://doi.org/10.5194/esurf-6-369-2018

Wang, Y., Liu, C., Zheng, D., Zhang, H., Yu, J., Pang, J., Li, C., Hao, Y., 2021. Multistage Exhumation in the Catchment of the Anninghe River in the SE Tibetan Plateau: Insights From Both Detrital Thermochronology and Topographic Analysis. Geophys Res Lett 48. https://doi.org/10.1029/2021gl092587

Whipple, K.X., 2009. The influence of climate on the tectonic evolution of mountain belts. Nature Geoscience 2, 97-104. https://doi.org/10.1038/ngeo413

Whipple, K.X., Forte, A.M., DiBiase, R.A., Gasparini, N.M., Ouimet, W.B., 2017. Timescales of landscape response to divide migration and drainage capture: Implications for the role of divide mobility in landscape evolution. Journal of Geophysical Research: Earth Surface 122, 248-273. https://doi.org/10.1002/2016JF003973

Whipple, K.X., Kirby, E., Brocklehurst, S.H., 1999. Geomorphic limits to climate-induced increases in topographic relief. Nature 401, 39-43. https://doi.org/10.1038/43375

Willett, S.D., McCoy, S.W., Perron, J.T., Goren, L., Chen, C.Y., 2014. Dynamic reorganization of river basins. Science 343, 1117. https://doi.org/10.1126/science.1248765

Wobus, C., Whipple, K.X., Kirby, E., Snyder, N., Johnson, J., Spyropolou, K., Crosby, B., Sheehan, D., 2006. Tectonics from topography: Procedures, promise, and pitfalls, Tectonics, Climate, and Landscape Evolution, pp. 55-74. https://doi.org/10.1130/2006.2398(04)

Xiong, L.-Y., Tang, G.-A., Li, F.-Y., Yuan, B.-Y., Lu, Z.-C., 2014. Modeling the evolution of loess-covered landforms in the Loess Plateau of China using a DEM of underground bedrock surface. Geomorphology 209, 18-26. https://doi.org/10.1016/j.geomorph.2013.12.009

Xu, X., Ma, X., Deng, Q., 1993. Neotectonic activity along the Shanxi rift system, China. Tectonophysics 219, 305-325. https://doi.org/10.1016/0040-1951(93)90180-R

Yan, M.-J., He, Q.-Y., Yamanaka, N., Du, S., 2014. Location, Geology and Landforms of the Loess Plateau, in: Tsunekawa, A., Liu, G., Yamanaka, N., Du, S. (Eds.), Restoration and development of the degraded Loess Plateau, China. Springer Japan, pp. 3-22. https://doi.org/10.1007/978-4-431-54481-4

Yang, R., Suhail, H.A., Gourbet, L., Willett, S.D., Fellin, M.G., Lin, X., Gong, J., Wei, X., Maden, C., Jiao, R., Chen, H., 2019. Early Pleistocene drainage pattern changes in Eastern Tibet: Constraints from provenance analysis, thermochronometry, and numerical modeling. Earth Planet Sc Lett 531, 1-10. https://doi.org/10.1016/j.epsl.2019.115955

Ye, Y., Tan, X., Zhou, C., 2022. Initial topography matters in drainage divide migration analysis: Insights from numerical simulations and natural examples. Geomorphology 409, 108266. https://doi.org/10.1016/j.geomorph.2022.108266

Yin, A., 2010. Cenozoic tectonic evolution of Asia: A preliminary synthesis. Tectonophysics 488, 293-325. https://doi.org/10.1016/j.tecto.2009.06.002

Zeng, X., Tan, X., 2023. Drainage divide migration in response to strike-slip faulting: An example from northern Longmen Shan, eastern Tibet. Tectonophysics 848, 229720. https://doi.org/10.1016/j.tecto.2023.229720

Zhao, X., Zhang, H., Hetzel, R., Kirby, E., Duvall, A.R., Whipple, K.X., Xiong, J., Li, Y., Pang, J., Wang, Y., Wang, P., Liu, K., Ma, P., Zhang, B., Li, X., Zhang, J., Zhang, P., 2021. Existence of a continental-scale river system in eastern Tibet

https://doi.org/10.5194/egusphere-2023-1428
Preprint. Discussion started: 11 August 2023

during the late Cretaceous-early Palaeogene. Nat Commun 12, 7231. https://doi.org/10.1038/s41467-021-27587-9

Zhou, C., Tan, X., Liu, Y., Lu, R., Murphy, M.A., He, H., Han, Z., Xu, X., 2022a. Ongoing westward migration of drainage divides in eastern Tibet, quantified from topographic analysis. Geomorphology 402, 108123. https://doi.org/10.1016/j.geomorph.2022.108123

Zhou, C., Tan, X., Liu, Y., Shi, F., 2022b. A cross-divide contrast index (C) for assessing controls on the main drainage divide stability of a mountain belt. Geomorphology 398, 108071. https://doi.org/10.1016/j.geomorph.2021.108071.

Zhou, C., Tan, X., 2023. Quantifying the influence of asymmetric uplift, base level elevation, and erodibility on cross-divide χ difference. Geomorphology 427, 108634. https://doi.org/10.1016/j.geomorph.2023.108634

Zondervan, J.R., Stokes, M., Boulton, S.J., Telfer, M.W., Mather, A.E., 2020. Rock strength and structural controls on fluvial erodibility: Implications for drainage divide mobility in a collisional mountain belt. Earth Planet Sc Lett 538. https://doi.org/10.1016/j.epsl.2020.116221